

Article

Enhanced Degradation of Ethylene in Thermo-Photocatalytic Process Using TiO₂/Nickel Foam

Maciej Trzeciak , Piotr Miądlicki  and Beata Tryba * 

Department of Catalytic and Sorbent Materials Engineering, Faculty of Chemical Technology and Engineering, West Pomeranian University of Technology in Szczecin, Pułaskiego 10, 70-322 Szczecin, Poland; maciej.trzeciak@zut.edu.pl (M.T.); piotr.miadlicki@zut.edu.pl (P.M.)

* Correspondence: beata.tryba@zut.edu.pl

Abstract: The photocatalytic decomposition of ethylene was performed under UV-LED irradiation in the presence of nanocrystalline TiO₂ (anatase, 15 nm) supported on porous nickel foam. The process was conducted in a high-temperature chamber with regulated temperature from ambient to 125 °C, under a flow of reacted gas (ethylene in synthetic air, 50 ppm, flow rate of 20 mL/min), with simultaneous FTIR measurements of the sample surface. Ethylene was decomposed with a higher efficiency at elevated temperatures, with a maximum of 28% at 100–125 °C. The nickel foam used as support for TiO₂ enhanced ethylene decomposition at a temperature of 50 °C. However, at 50 °C, the stability of ethylene decomposition was not maintained in the following reaction run, but it was at 100 °C. Photocatalytic measurements conducted in the presence of certain radical scavengers indicated that a higher efficiency of ethylene decomposition was obtained due to the improved separation of charge carriers and the increased formation of superoxide anionic radicals, which were formed at the interface of the thermally activated nickel foam and TiO₂.

Keywords: thermo-photocatalysis; TiO₂/nickel foam; ethylene decomposition; superoxide anionic radicals



Citation: Trzeciak, M.; Miądlicki, P.; Tryba, B. Enhanced Degradation of Ethylene in Thermo-Photocatalytic Process Using TiO₂/Nickel Foam. *Materials* **2024**, *17*, 267. <https://doi.org/10.3390/ma17010267>

Academic Editor: Salvatore Scire`

Received: 21 November 2023

Revised: 11 December 2023

Accepted: 14 December 2023

Published: 4 January 2024



Copyright: © 2024 by the authors. Licensee MDPI, Basel, Switzerland. This article is an open access article distributed under the terms and conditions of the Creative Commons Attribution (CC BY) license (<https://creativecommons.org/licenses/by/4.0/>).

1. Introduction

Ethylene, which belongs to the group of volatile organic compounds (VOCs), is a naturally occurring gas that is emitted by plants. As a phytohormone, ethylene has both desirable and undesirable effects on the storage of fresh vegetables and fruits [1]. It plays a crucial and beneficial role in the development of distinctive colour, taste and flavours in fresh produce. Conversely, the accumulation of ethylene in plants induces premature ripening, senescence and ageing, resulting in a faster deterioration and a shortening of shelf life [2,3].

The effective removal of ethylene from these areas is therefore crucial, and a myriad of strategies have been employed to degrade it. Methods for ethylene degradation vary, spanning from biological processes involving the use of various types of biofilters [2,4], the employment of sorbents such as zeolites or activated carbon [1,5] and the application of air ventilation or air filtration dependent on catalytic oxidation [6,7]. However, these methods often face challenges in terms of efficiency, selectivity and operational conditions.

Amidst these diverse strategies, photocatalytic degradation is a viable substitute for mitigating ethylene-induced spoilage. This innovative approach utilises light in the ultraviolet-to-visible spectrum to activate a photocatalyst, namely, titanium dioxide (TiO₂), which can oxidise ethylene molecules into less harmful compounds [7]. Unlike traditional methods, photocatalysis can be conducted at room temperature and atmospheric pressure, making it an environmentally friendly option that can be used in various settings. Photocatalysis also offers tailored solutions that can optimise the degradation of ethylene according to the unique needs of different storage facilities [6–8].

Numerous studies have demonstrated the effectiveness of TiO₂ in the photocatalytic decomposition of ethylene, highlighting its potential as a reliable and efficient method for reducing ethylene concentration. In the work of Park et al. [9], ethylene photodegradation was investigated using ultrafine powdered TiO₂ in the presence of water vapor and O₂. In a different paper [8], novel titania nanoparticles were successfully used for the decomposition of ethylene under cold storage conditions.

While the use of titanium dioxide (TiO₂) in the photocatalytic degradation of ethylene presents a promising eco-friendly alternative, it is not without its shortcomings. Foremost among these is the recombination of electron–hole pairs within TiO₂. This significantly diminishes its photocatalytic efficiency. Furthermore, TiO₂'s ability to absorb visible light is constrained due to its large bandgap, specifically 3.2 eV in the anatase phase, which necessitates the use of ultraviolet light for efficient photocatalytic performance. This is significant since UV light comprises only about 5% of the sun's emissions [10]. Thus, utilising UV light can be both costly and energy-intensive. To mitigate these limitations, UV-LEDs can be employed, which are reported [11] to have a higher energy efficiency, more consistent light intensity and longer lifetime than traditional UV lamps, thereby enhancing the efficiency and sustainability of the photocatalytic process. In a study conducted by Fonseca et al. [12], ethylene decomposition using TiO₂ in a NETmix mini-photoreactor was investigated, with illumination provided by UVA-LEDs. Such an approach seems to be a better solution than the modification of TiO₂ for achieving its visible light activity because visible light is less energetic than UV and results in a lower quantum yield of the photocatalytic degradation process. Additionally, as reported elsewhere [13], ethylene molecules display a low adsorption capacity and photodegradation rate on the (001) surface of titania, which is considered the most reactive for surface-catalysed reactions. The weak adsorption energy of ethylene signifies its negligible interaction with the TiO₂ surface, presenting a significant challenge in the design of efficient photocatalytic materials, as strong adsorbate–surface interactions are critical for optimal performance [13,14].

Addressing these limitations, a variety of methods have been investigated aiming to enhance the photocatalytic performance of TiO₂. One of the methods commonly used to enhance the efficiency of TiO₂ is the doping of some species, which can change its wide bandgap, improve visible light absorption and reduce electron–hole recombination [15]. Doping can be achieved using elements such as metals (transition [16], rare-earth [17] and noble [18]) and non-metals (N [19], C [20], S [21] and others) or co-doping, which involves the simultaneous introduction of multiple dopants [15,22]. Another approach used for increasing the photocatalytic activity of TiO₂ is changing its morphology. Kajita et al. [23] prepared a thin-film TiO₂ with fibreform nanostructures using helium plasma treatment. They proved that, in such a formed nanostructure, the presence of both oxygen vacancies and the dominant anatase phase determines its high photocatalytic activity towards ethylene decomposition. Another promising approach involves the development of new composite photocatalysts. Metal–organic frameworks (MOFs) are crystalline materials composed of metal clusters coordinated to organic ligands. MOFs possess unique characteristics, particularly a large specific surface area, high pore volume and alterable pore size, which contribute positively to the efficiency of photocatalysis and the adsorption of gases [24]. As stated in [25], a photocatalytic system made of a combination of TiO₂, MIL101(Fe) and reduced graphene oxide (rGO) successfully enhanced the separation efficacy of electron–hole pairs and improved gas adsorption capacity. In other studies [26], the researchers explored the possibilities of combining rGO with black TiO₂ nanosheets, which resulted in a significant increase in both visible light absorption and the adsorption of ethylene on the composite surface. In this way, they obtained enhanced photocatalytic efficiency using this new material. Recent research studies have also revealed the emergence of photocatalysts combined with nickel foam as novel composite materials in the field of the photocatalytic degradation of VOCs. Nickel foam stands out for its high porosity, excellent conductivity and affordability, making it particularly useful for photocatalytic systems [27]. It has been previously reported that TiO₂ combined with nickel foam can

be used for the photocatalytic degradation of various pollutants, including toluene [28], formaldehyde [29] and acetaldehyde [30–32]. As stated in our previous paper [31], nickel foam used in combination with TiO₂ considerably enhanced charge separation in TiO₂ and positively affected the formation of superoxide anion radicals, which were utilised in photocatalytic reactions.

The objective of this study was to investigate the decomposition of ethylene in the presence of nanocrystalline TiO₂, which was loosely loaded on nickel foam. The impact of nickel foam on photocatalytic efficacy was investigated. The photocatalytic process was carried out at various temperatures, from 25 to 125 °C, and under UV light irradiation emitted by UV-LEDs. Studies on reactive radicals engaged in ethylene decomposition were performed using some radical scavengers.

2. Materials and Methods

2.1. Characteristics of Materials

2.1.1. Methods

The experiments of ethylene decomposition in a thermo-photocatalytic system were carried out by employing a high-temperature reaction chamber (Praying Mantis, Harrick, Pleasantville, NY, USA), as reported in our previous paper [31]. Throughout the experimental procedure, continuous Fourier transform infrared (FTIR) measurements were conducted using a Thermo Nicolet iS50 FTIR instrument (Thermo, Waltham, MA, USA). Spectra were collected in the range of 1200–1400 cm⁻¹ with a resolution of 4 cm⁻¹, with each spectrum consisting of 40 scans. KBr was used for the background. Spectra were collected every minute for 300 min. UV irradiation was applied through a quartz window utilising an illuminator equipped with fibre optics and a UV-LED 365 nm diode with an optical power of 415 mW (LABIS, Warszawa Poland). The intensity of incident UV radiation was measured using a photo-radiometer, HD2102.1 (TEST-THERM, Kraków, Poland). The obtained UV intensity value measured on the surface of the reactor cover window equalled 20 W/m². The model gas of ethylene (C₂H₄ 50 ppm in synthetic dry air, Air Liquide, Kraków, Poland) was supplied through an inlet regulated by a mass flow meter. The applied flow rate of the ethylene gas was 20 mL/min, and this was selected based on preliminary studies, taking into account the highest quantity of decomposed ethylene molecules in time. The calculated value of GHSV was 10,620 h⁻¹. The concentration of ethylene was determined in a gas chromatograph with a flame ionisation detector (GC-FID, SRI, Menlo Park, CA, USA). A calibration curve was prepared using a calibration gas with an ethylene concentration of 50 ppm in synthetic air. Analyses were carried out under the following conditions: isothermal oven temperature of 60 °C; detector temperature of 250 °C; automatic sampling loop volume of 2 mL; and a metal capillary column (MXT-1301) of 15 m, with an ID of 0.53 mm and 3.00 µm.

Figure 1 presents a photo of the Praying Mantis™ high-temperature reaction chamber with a Diffuse Reflection Accessory mounted on the IR spectrometer, together with the UV-LED source and its emission spectrum.

A powdered TiO₂ sample was loosely poured onto nickel foam (without any binder), and this prepared mixture was placed inside the reaction chamber. TiO₂ particles filled up the cavities of the nickel foam. The reacted gas flowed from the top to the bottom of the reactor, and then it was directed to the GC-FID equipped with an automatic dozen loop and analysed every 5 min during the ongoing process. Measurements were also carried out in the presence of only TiO₂, without nickel foam.

TiO₂ was analysed through XRD measurements using a diffractometer (PANalytical, Almelo, The Netherlands) equipped with a Cu X-ray source ($K_{\alpha 1} = 0.154056$ nm, $K_{\alpha 2} = 0.154439$ nm). K_{β} was removed with a Ni filter, while $K_{\alpha 2}$ was removed with the numerical procedure of the Rachinger method. The measurements were performed in the 2θ range of 20–90°, with a step size of 0.013. A voltage of 35 kV and a current of 30 mA were applied. Philips HighScore plus software 3.0.5. (Pdf4+ database) was used for phase identification. The content of the anatase phase, X_A , was determined from the integrated

intensity of the (101) diffraction line of the anatase phase (I_A) and that of the (110) line of the rutile phase (I_R), using the following equation [33]:

$$X_A = 0.75 \times I_A / (I_R + 0.75 \times I_A) \quad (1)$$

The formula was obtained by using the reference intensity ratio (RIR) factors from the PDF-4+ database. The cards of reference codes 01-088-117 and 01-071-1168 were used for rutile and anatase, respectively.

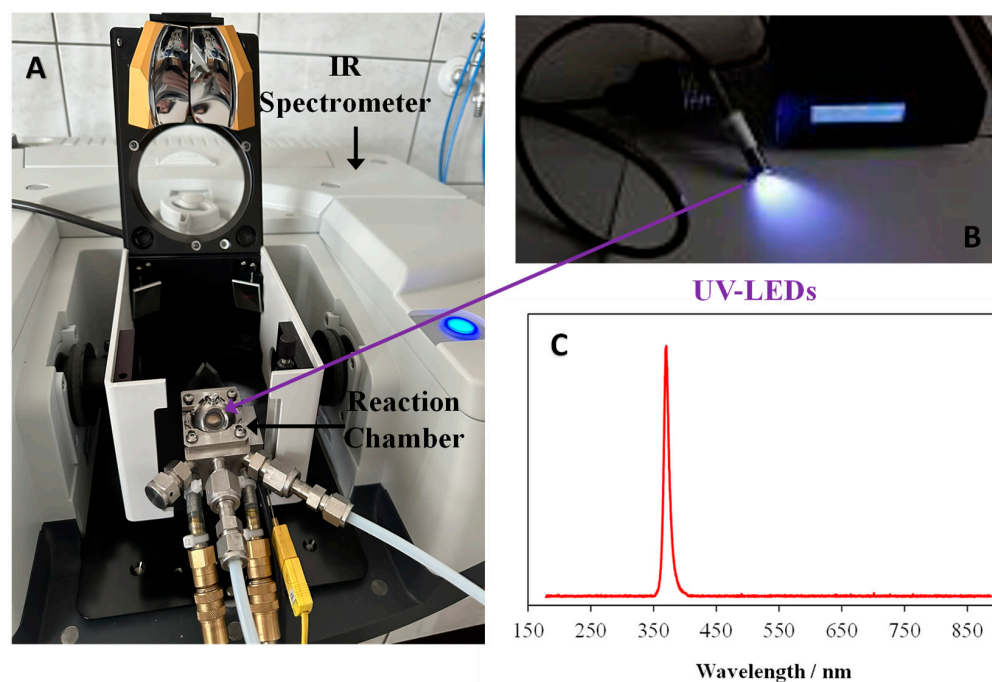


Figure 1. (A) Praying Mantis™ Diffuse Reflection Accessory with high-temperature reaction chamber in FTIR spectrometer. (B) The optical fibre with UV LED diode; (C) the emission spectrum of UV LED diode.

The average crystallite size of anatase was calculated based on the Scherrer formula:

1. $d = K \times \lambda / (B - b) \times \cos\theta$, where:
2. d —the average crystallite size;
3. K —the shape factor;
4. λ —the X-ray wavelength;
5. B —the line width measured at FWHM, originating both from crystallite sizes and instrumental broadening;
6. b —the line width originating solely from instrumental broadening;
7. h —the reflex position.

A shape factor of 0.94 was assumed, and the broadening of the reflex originated solely from the instrumental broadening and the size of the crystallites. The instrumental broadening was estimated using the measurement of the silicon reference sample. The determined value of the instrumental broadening for the anatase (101) and the rutile (110) positions was found to be 0.086.

The specific surface area of TiO_2 was determined from the nitrogen adsorption/desorption isotherms measured at 77 K using a QUADRASORB Si analyser (Quantachrome, Boynton Beach, FL, USA). Before measuring, the sample was degassed at 105 °C for 12 h under high vacuum using a MasterPrep degasser by Quantachrome. The BET surface area was calculated using the BJH method.

The morphologies of the nickel foam and powdered TiO_2 were analysed using FE-SEM in a Hitachi SU8020 SEM with field cold emission.

To identify the dominant species participating in the photocatalytic reactions, measurements were performed in the presence of hole, hydroxyl radicals and oxygen radical scavengers. Terephthalic acid, ethylenediaminetetraacetic acid (EDTA) and p-benzoquinone were used to trap $\bullet\text{OH}$, h^+ and $\text{O}_2^{\bullet-}$ species, respectively. The applied procedure followed the methodology reported by Q. Zeng et al. [34] and involved a mixture of 0.1 g TiO_2 with 0.01 g of each scavenger individually. The mixture was then loaded onto purified nickel foam and tested. An excess of scavenger was used to ensure the entire capture of demanded radicals. The decomposition of ethylene in the presence of TiO_2 and scavenger was carried out at 100 °C under UV irradiation in a high-temperature chamber. As a control test, a mixture of 0.1 g TiO_2 and 0.01 g KBr was used, because KBr has been known to be chemically inert for ethylene gas and is transparent for IR.

2.1.2. Materials

TiO_2 was synthesised through a two-step procedure: an initial hydrothermal treatment of titania pulp (obtained from Police Chemical Factory, Police, Poland) in deionised water at 150 °C and 7.4 bar for 1 h. Subsequently, the resultant mixture underwent decantation, followed by drying at 100 °C, and then it was subjected to a tube furnace under an argon flow of 30 mL/min (heating rate: 10 °C/min) until reaching 400 °C, where it was maintained for 2 h.

The nickel foam (sourced from Jiujiang Xingli Beihai Composite Co., Ltd., Jiujiang, China) exhibited a purity of 99.8%. It possessed the following specifications: a thickness of 1.5 mm, porosity ranging between 95% and 97%, and a surface density of 300 g/m².

The chemicals utilised in the studies included p-benzoquinone (with HPLC-grade purity of over 99.5%, sourced from Fluka Analytical in Darmstadt, Germany), terephthalic acid (TA) (with a purity of 98%, obtained from Sigma-Aldrich in Saint Louis, MO, USA) and ethylenediaminetetraacetic acid (EDTA) (Pure Chemical Standards-Elemental Microanalysis, Okehampton, UK).

3. Results

3.1. Physicochemical Properties of TiO_2

The XRD pattern of the prepared TiO_2 sample is shown in Figure 2. The primary crystalline phase observed in the TiO_2 sample was anatase. Low-intensity signals assigned to the rutile phase were also observed. The calculation of the average crystallite size of anatase was performed based on the Scherrer equation. The calculated size of anatase crystallites equalled approximately 15 nanometres. The performed calculations of the phase composition indicated that the share of rutile in this TiO_2 was around 4 wt%. The measured BET surface area of TiO_2 equalled 167 m²/g.

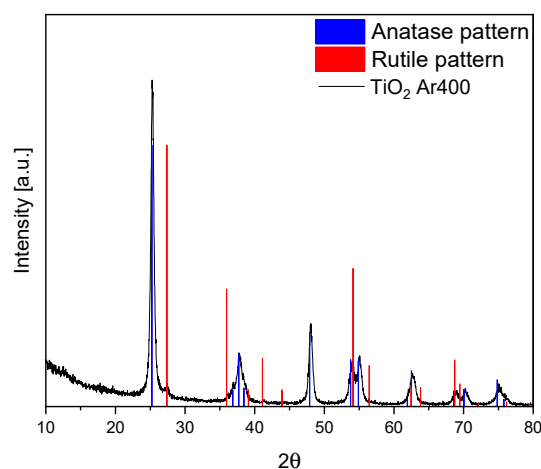


Figure 2. XRD pattern of TiO_2 and patterns representing the standard diffraction data from the JCPDS file for anatase (No. 01-071-1168) and rutile (No. 01-088-117).

Figure 3 presents SEM images of the nickel foam at various magnifications.

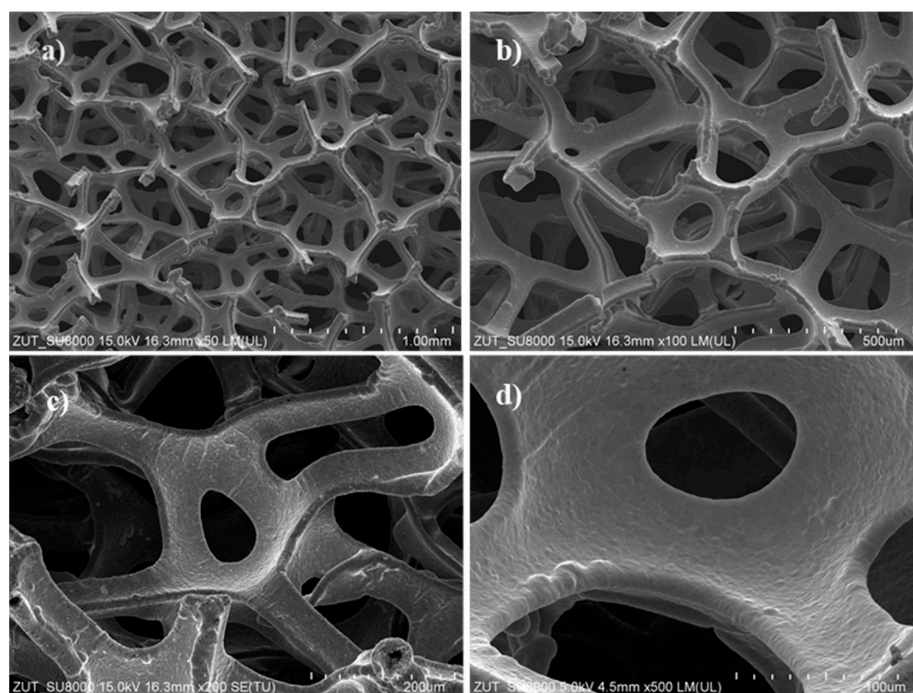


Figure 3. SEM images of nickel foam at different magnifications: (a) 50, (b) 100, (c) 200 and (d) 500 times.

The structure of the nickel foam appears to be very porous, containing multilayered sheets with irregular cavities ranging in size from a few tens to a few hundred micrometres. The overall texture resembles a juxtaposition of polygonal cavities.

In Figure 4, the morphology of the TiO_2 powder is presented in SEM images taken at various magnifications.

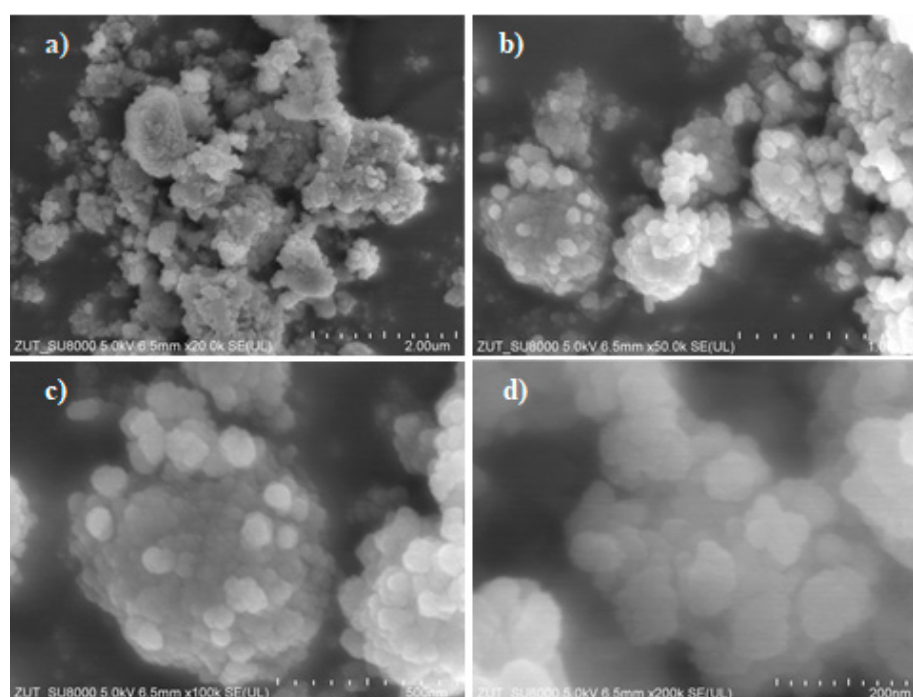


Figure 4. SEM images of TiO_2 powder at different magnifications: (a) 20, (b) 50, (c) 100 and (d) 200 times.

The TiO₂ structure resembles branches of fine flakes interconnected with each other. Small titania particles with a size of around 100 nm are observed, and they form the agglomerates of a larger size.

3.2. Thermo-Photocatalytic Decomposition of Ethylene in the Presence of TiO₂ and TiO₂/Nickel Foam under UV-LED Light

The results of the thermo-photocatalytic decomposition of ethylene under UV-LED illumination in the presence of TiO₂ supported on KBr are shown in Figure 5. The percentage of ethylene decomposition ranged from about 18% at 25 °C to about 28% at 100–125 °C. Higher temperatures in the photocatalytic process resulted in slightly higher ethylene decomposition. Fluctuations in ethylene removal were observed during the period of UV irradiation.

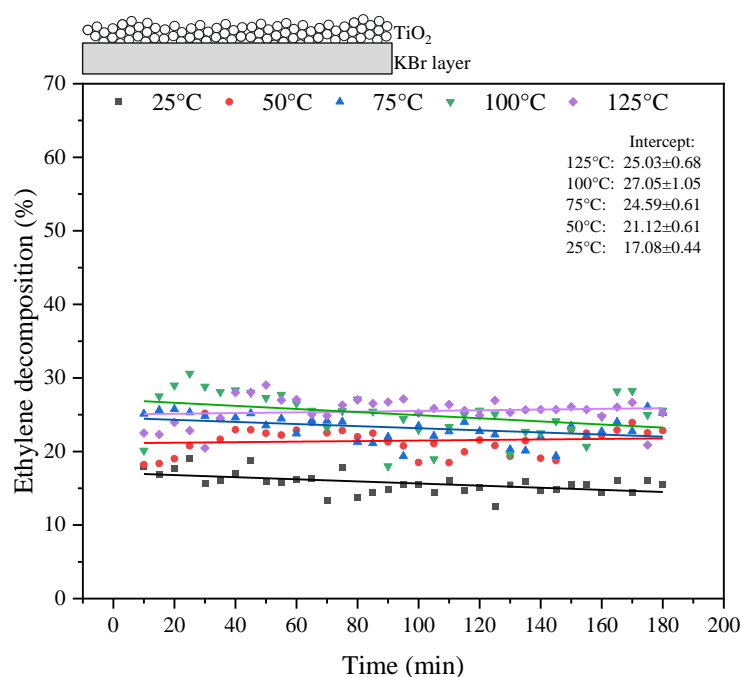


Figure 5. Photocatalytic decomposition of ethylene under UV irradiation at various reaction temperatures in the presence of TiO₂/KBr.

In the next step, TiO₂ was supported on the nickel foam, and the photocatalytic process of ethylene decomposition was repeated. The results from the performed experiments are shown in Figure 6. A high increase in ethylene decomposition was observed when the process was carried out at elevated temperatures, with the maximum yield (50%) being achieved at temperatures of 100–125 °C. The yields of the photocatalytic reactions decreased with time as the process progressed; however, at 100–125 °C, they reached a certain stability after 60 min, with only about a 5% drop in efficacy. The blind test of ethylene decomposition in the presence of UV and nickel foam was performed at various temperatures (up to 300 °C), and the results indicate that ethylene did not decompose in the absence of TiO₂. A similar test was carried out for an empty reactor, and, again, these measurements indicate that ethylene was stable under UV and heating until 300 °C.

3.3. Thermo-Photocatalytic Decomposition of Ethylene in the Presence of Radical Scavengers

Some radical scavengers were added to TiO₂ in order to examine the share of the formed reactive radicals in the photocatalytic reactions related to the decomposition of ethylene. The process was carried out at 100 °C in the presence of TiO₂ mixed with a scavenger and poured on nickel foam. The obtained results are presented in Figure 7.

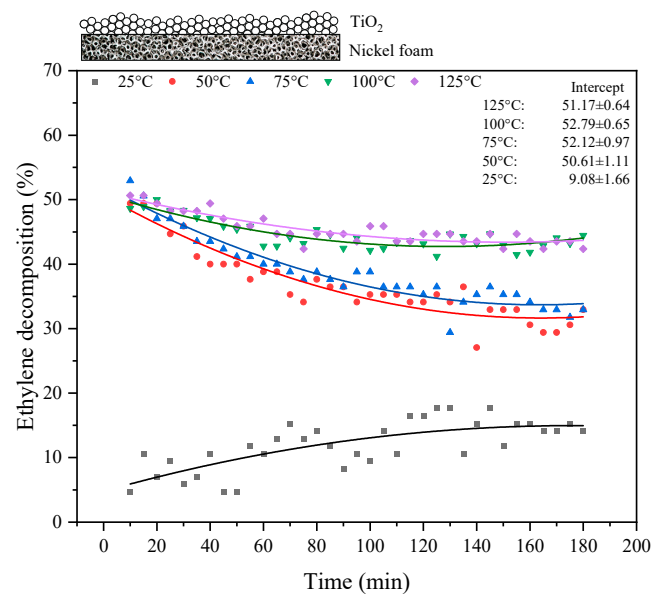


Figure 6. Photocatalytic decomposition of ethylene under UV irradiation at various reaction temperatures in the presence of TiO₂/nickel foam.

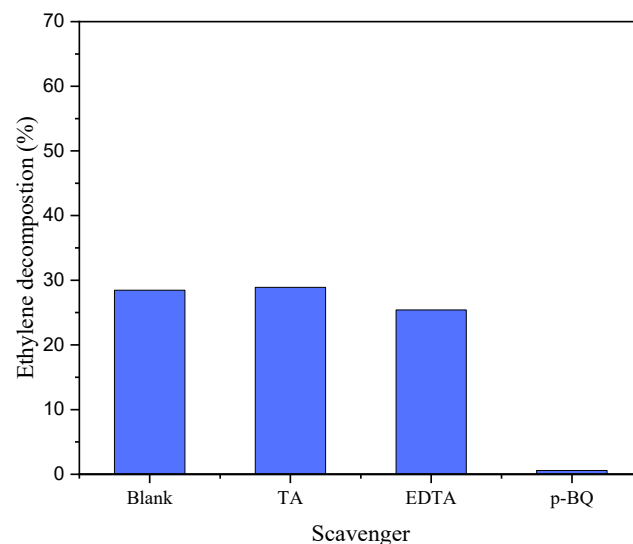


Figure 7. Photocatalytic decomposition of ethylene in the presence of TiO₂/nickel foam at 100 °C with the addition of some radical scavengers.

After adding terephthalic acid (TA) to TiO₂, a scavenger of hydroxyl radicals, the decomposition of ethylene was unchanged compared to the blank test with TiO₂ only. However, when EDTA, a hole scavenger, was added to TiO₂, the degradation of ethylene decreased slightly. The introduction of p-benzoquinone (p-BQ), acting as a scavenger for superoxide anion radicals, caused the almost complete inhibition of the photocatalytic process. These experiments demonstrate that superoxide anion radicals played the leading role in the process of ethylene degradation.

3.4. FTIR Spectra of the Photocatalyst Surface Measured at the Condition of the Photocatalytic Process of Ethylene Decomposition

Figures 8–10 show FTIR spectra illustrating the interaction of ethylene with the titania surface during thermo-photocatalytic processes. In situ, diffuse reflectance infrared Fourier transform spectroscopy (DRIFTS) was applied. The FTIR spectra presented in Figure 8 illustrate the changes in the chemical structure of the TiO₂ surface when exposed

to ethylene gas (50 ppm in air), UV irradiation and thermal heating. The starting TiO₂ material contained hydroxyl groups, as indicated by the FTIR bands at 3690 and 1620 cm⁻¹ assigned to OH groups and those at 3700–2500 cm⁻¹ assigned to molecular adsorbed water. During the photocatalytic process of ethylene decomposition conducted at an increased temperature, some new bands appeared. At 25 °C, a strong band at 3740 cm⁻¹ was observed together with another broad and weak band at 3650 cm⁻¹. At the same time, the intensity of the broad band at 3700–2500 cm⁻¹ diminished. According to Park et al. [9], the band at 3740 cm⁻¹ is attributed to OH groups adsorbed on the TiO₂ surface and is formed after the desorption of physically adsorbed water molecules, which can be observed through the reduction in the intensity of the band at 3700–2500 cm⁻¹. The band at 3650 cm⁻¹ is also attributed to OH groups adsorbed on the TiO₂ surface, but on the other site. According to Bhattacharyya et al. [16], such bonded OH groups are highly responsible for dihydroxylation and can participate in the formation of CH₃-CH₂-O⁻ species. While the band at 3740 cm⁻¹ was clearly observed only at 25 °C, the other at 3650 cm⁻¹ showed an increase with rising reaction temperatures. The conducted process of ethylene decomposition revealed that the bands assigned to hydroxyl groups at 3650 and 3740 cm⁻¹ appeared and disappeared in the FTIR spectra over the course of the reaction. It is therefore speculated that the formation of CH₃-CH₂-O⁻ species, as well as hydroxyl radicals involving these OH groups, is highly plausible. Newly appeared bands at 1542 and 1340 cm⁻¹ were observed at higher temperatures, such as 50–150 °C, and they can be attributed to the C=C stretching vibrations and -CH₂ symmetric scissoring vibrations of adsorbed ethylene, respectively [16]. These studies indicate that the adsorption of ethylene could be increased at higher reaction temperatures, while the extensive hydroxylation of the titania surface has a negative effect on the adsorption of ethylene. It has been reported in the literature [35] that ethylene is less strongly adsorbed onto the TiO₂ surface than water. The negative impact of the high adsorption of water molecules on the TiO₂ surface during ethylene decomposition has also been observed by other researchers [16]. Therefore, the decomposition of ethylene under UV irradiation at 25 °C was significantly lower than that at elevated temperatures. The lower adsorption of ethylene on the titania surface resulted in a lower degree of decomposition. Table 1 lists some identified functional groups present on the TiO₂ surface during the photocatalytic process of ethylene decomposition.

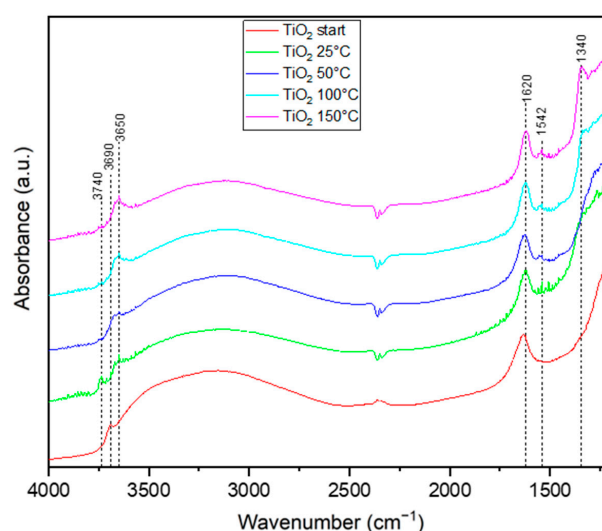


Figure 8. In situ FTIR spectra of titania surface during the photocatalytic decomposition of ethylene using TiO₂.

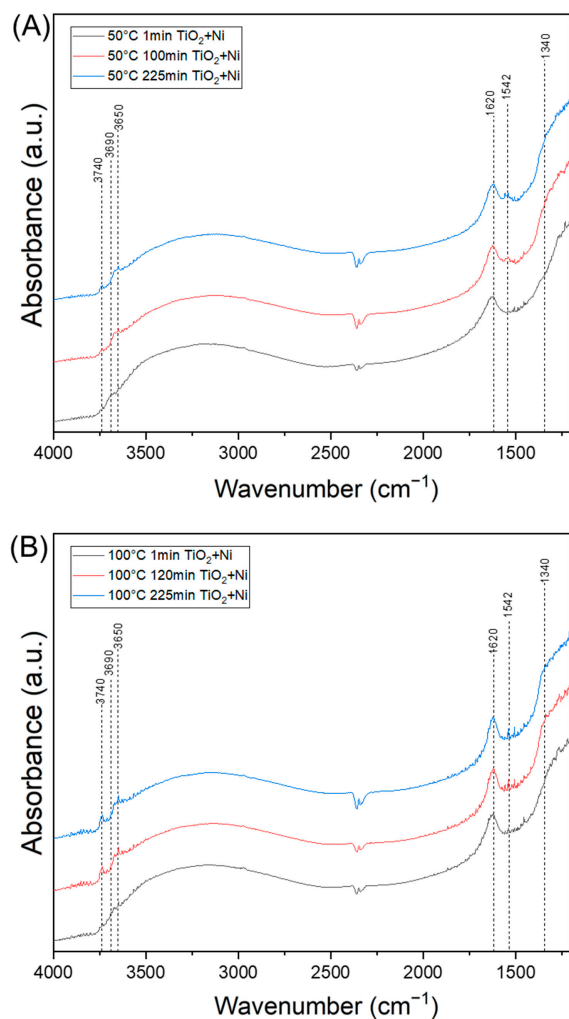


Figure 9. In situ FTIR spectra of titania surface recorded during the photocatalytic decomposition of ethylene using TiO₂/nickel foam (A) at 50 °C and (B) at 100 °C.

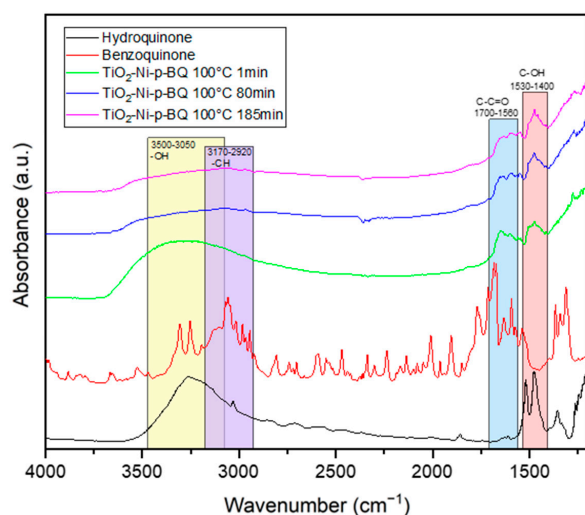


Figure 10. In situ FTIR spectra of titania surface during the photocatalytic decomposition of ethylene using TiO₂-p-BQ/nickel foam at 100 °C.

Table 1. Characteristics of FTIR bands.

Functional Group	Wavenumber (cm ⁻¹)	References
C=C C=O	1542	[16]
-CH ₂	1340	[16]
H ₂ O	2500–3600	[16]
-OH	3740, 3690, 3650	[14,16]
-OH	1620	[14]

Figure 9 shows FTIR spectra that illustrate the changes in the chemical surface of titania when loaded on nickel foam and subjected to photocatalytic ethylene decomposition at temperatures of 50 and 100 °C. These FTIR spectra were recorded at various times during the photocatalytic process (1 min, 120 and 225 min). At 50 °C, new bands became clearly visible at 1542 and 1360 cm⁻¹ as the photocatalytic process progressed, while the other bands at 1340 cm⁻¹ and 3650 cm⁻¹ were also subtly visible. At 100 °C, the most intensive band was observed at 3740 cm⁻¹, but the band at 1542 cm⁻¹ was poorly visible due to the high noise of the spectral signals. The band at 1542 cm⁻¹ can be assigned to C=C vibrations in the adsorbed ethylene, as described earlier, or it can be a result of ν(C=O) vibrations in the acetate ions (COO⁻) formed as the product of ethylene transformation [9,14]. Taking into account that, at 50 °C, the percentage of ethylene decomposition decreased with the increasing time of UV irradiation, it is stated that the band at 1542 cm⁻¹ is related to some acetate species, byproducts of ethylene decomposition. According to some researchers [9], these species can be strongly held on the TiO₂ surface. In our previous studies [14], some acetate species were also identified on the TiO₂ surface upon ethylene decomposition with a higher dose of 200 ppm. Therefore, it can be concluded that, at 50 °C, TiO₂ surface deactivation occurred over time due to the incomplete decomposition of ethylene. In contrast, at 100 °C, this process was insignificant, and a high adsorption of OH groups was observed on the titania surface (band at 3740 cm⁻¹), likely resulting from ethylene mineralisation. These adsorbed OH ions on the TiO₂ surface may contribute to hydroxyl radical formation, thereby enhancing the mineralisation of ethylene species. A similar effect was observed by Park et al. [9].

In the next step, the mechanism of the p-BQ reaction with superoxide anionic radicals, which were formed on the TiO₂/nickel foam, was studied in the presence of ethylene gas (50 ppm in the air) under UV-LED irradiation. The measurements were conducted at 25 and 100 °C. The obtained FTIR spectra, recorded at the beginning and after 80 and 185–200 minutes of the thermo-photocatalytic process, are presented in Figures 10 and 11. It was clearly observed that, with the increasing time of the reaction, p-BQ converts to hydroquinone (HQ). This conversion was evidenced by a decrease in the intensity of the bands at 1560–1700 cm⁻¹ (assigned to the -C-C=O groups in p-BQ), with a simultaneous increase in the intensity of the bands at 1530–1400 cm⁻¹ (corresponding to the OH groups in HQ). Additionally, the hydroxyl groups originally present on the TiO₂ surface are consumed over time during the reactions (indicated by the band at 2700–3600 cm⁻¹). Furthermore, at 25 °C (Figure 11), a significant increase in the intensity of OH groups was observed in the 3500–3050 and 1530–1400 cm⁻¹ ranges, attributed to HQ [36,37]. There is a high likelihood that p-BQ undergoes photolysis under UV irradiation and water, leading to the formation of 1,2,4-trihydroxybenzene (1,2,4-THB), which is then further oxidised to HQ. This mechanism has been previously reported in the literature [38]. A high increase in the intensity of the band at 3500–3050 cm⁻¹ can be a result of the overlapping of both spectra, 1,2,4-THB and HQ. This phenomenon was not observed at 100 °C. It is stated that, at 25 °C, under UV irradiation, the desorption of physically bound water molecules from the titania surface occurs, participating in the p-BQ photolysis reaction. At 100 °C, the titania surface is less hydroxylated than at ambient temperature, suggesting that the mechanism of p-BQ

conversion to HQ might follow a different pathway. In the absence of water, p-BQ can be transformed to HQ through the photocatalytic reaction with TiO_2 involving scavenging electrons or superoxide anionic radicals [38]. These reactions depend on the presence of oxygen and the pH of the solution. In our studies, the application of p-BQ as a scavenger significantly suppressed ethylene decomposition. It is concluded that superoxide anionic radicals play an important role in the photocatalytic process of ethylene decomposition.

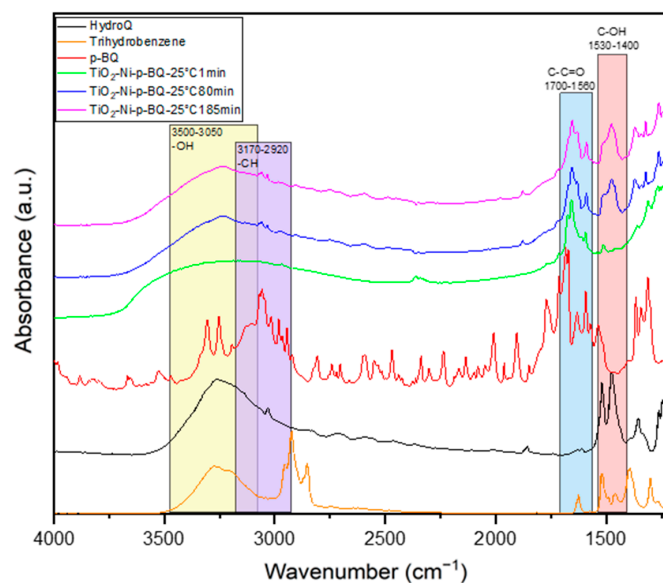


Figure 11. In situ FTIR spectra of titania surface during the photocatalytic decomposition of ethylene using TiO_2 -p-BQ/nickel foam at 25 °C.

The FTIR spectra of the titania surface, measured during ethylene decomposition in the presence of EDTA (used as the hole scavenger, Figure 12), indicate that the adsorption of hydroxyl groups on TiO_2 (evident from the band at 3740 cm^{-1}) was lower than in the case of using only TiO_2 . However, other OH groups at 3650 cm^{-1} appeared. The scavenging of holes by EDTA led to a reduced attraction of some OH groups to the titania surface, consequently leading to the formation of fewer hydroxyl radicals. However, the presence of a band at 3650 cm^{-1} can be evidence that OH groups are adsorbed on the other side of TiO_2 . There is no direct evidence identifying which adsorbed OH groups take part in the formation of hydroxyl radicals. However, it is assumed that the scavenging of holes by EDTA decreased the yield of ethylene removal due to the suppression of hydroxyl radical formation. This process should be studied in detail in further research work.

Contrary to that, the addition of terephthalic acid (TA) to TiO_2 did not result in any changes in the yield of the photocatalytic system. The recorded FTIR spectra (Figure 13) of the TiO_2 surface during the photocatalytic process showed no visible changes in the structure of TA. It is suggested that the reaction of TA with OH radicals, formed upon TiO_2 excitation, was hindered due to the low mobility of these radicals and potential lack of contact. In an aqueous medium, the situation differs, as hydroxyl radicals can easily desorb from the titania surface and participate in photocatalytic reactions.

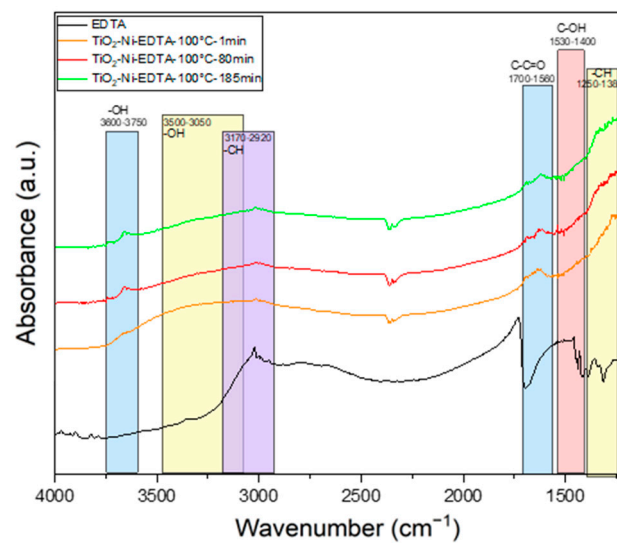


Figure 12. In situ FTIR spectra of titania surface during the photocatalytic decomposition of ethylene using TiO_2 -EDTA/nickel foam at $100\text{ }^\circ\text{C}$.

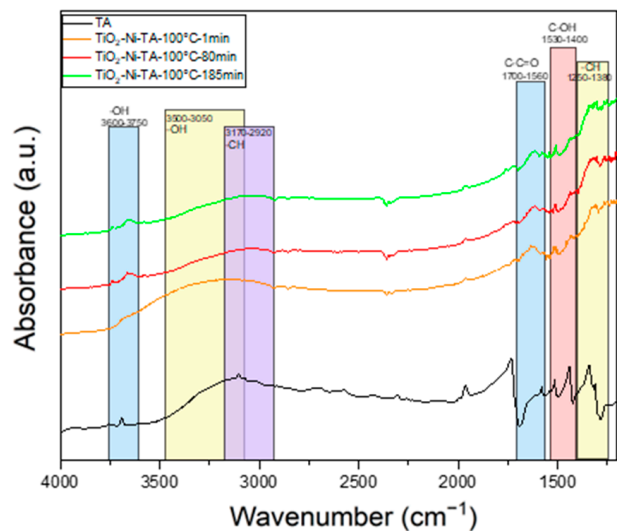


Figure 13. In situ FTIR spectra of titania surface during the photocatalytic decomposition of ethylene using TiO_2 -TA/nickel foam at $100\text{ }^\circ\text{C}$.

4. Discussion

TiO_2 mounted on nickel foam can be a sufficient photocatalyst for ethylene decomposition when the reaction is conducted under UV and at elevated temperatures, such as $100\text{ }^\circ\text{C}$. At ambient temperature, TiO_2 , whether supported on Ni foam or not, appeared to have the lowest activity. The mobility of the electrons at this temperature was most likely lower than in the case of thermal conditions, and, moreover, physically adsorbed water molecules on the titania surface could participate in speeding up the recombination process. A certain amount of hydroxyl groups adsorbed on the titania surface is beneficial because they can take part in the reaction with photogenerated holes to form hydroxyl radicals. However, a high hydroxylation of the TiO_2 surface leads to the suppression of oxygen uptake by photogenerated electrons and limits the formation of oxygen radicals [9]. The measurements of ethylene decomposition carried out in the presence of radical scavengers showed that superoxide anionic radicals played the main role in the photocatalytic decomposition of ethylene. The highest yield of ethylene decomposition was achieved for the process conducted at $100\text{ }^\circ\text{C}$ in the presence of TiO_2 mounted on nickel foam, where almost no deactivation occurred, the process was stable for 60 min, and a decrease in

ethylene decomposition of about 5% was observed during the first 60 min of UV irradiation. Promising results were obtained because the activation of the nickel foam occurred at 100 °C, where, most likely, the mobility of the electrons increased, and some superoxide anionic radicals formed at the interface of the Ni foam and TiO₂. It is assumed that the nickel foam improved the separation of free charges and enhanced the formation of reactive radicals. L. Chen et al. postulated that superoxide anionic radicals played a key role in the photocatalytic decomposition of ethylene [25]. Other researchers investigated the formation of oxygen radicals upon ethylene decomposition in air and UV irradiation using the EPR technique [9]. Initially, they observed the formation of hydroxyl radicals and Ti³⁺ centres, whereas, later on, O₂^{•−} radicals appeared together with O₃^{•−}. The authors explained that O₃^{•−} radicals were formed through the reaction of hole trapping with oxygen and O₂^{•−} radicals by oxygen adsorption on Ti³⁺ centres [9]. Our studies showed certain activity of photogenerated holes in ethylene decomposition. There is a certain probability that both O₂^{•−} and O₃^{•−} radicals are formed upon the photocatalytic process.

In general mechanism of ethylene decomposition at the presence of TiO₂ and nickel foam can be described by the following reactions:

- under UV irradiation some hole and electrons species are formed in TiO₂, which are utilized in the reactions:



- hole traps (O^{•−}) can react with adsorbed C₂H₄ to form (C₂H₄O)[•], which undergoes further mineralisation to CO and CO₂:



- hole traps can be also transformed to O₃^{•−} in the reaction with oxygen:



- the presence of nickel foam increases separation of e[−]/h⁺ pairs in TiO₂ giving higher yield in the photocatalytic reactions and also increases the electron traps in TiO₂. Therefore in combination of TiO₂ and nickel foam there is boosting of superoxide anionic radicals, which greatly contribute in the photocatalytic mineralisation of ethylene:



- formed H₂O upon C₂H₄ decomposition can be adsorbed on TiO₂ surface and take parts in the further process of photocatalytic reactions.

These studies show the beneficial effect of using TiO₂ supported on nickel foam when the process is carried out at 100 °C. The separation of charge carriers in TiO₂, the dehydro-ylation of the surface and the formation of superoxide anionic radicals are the most important issues for the effective decomposition of ethylene in air.

5. Conclusions

The application of TiO₂ supported on nickel foam can enhance the photocatalytic decomposition of ethylene under UV-LED irradiation and an increased temperature of up to 100 °C. It was confirmed that an increase in the temperature of the photocatalytic process leads to the activation of nickel foam and TiO₂ and causes an enhanced generation of superoxide anionic radicals, which takes place in ethylene decomposition. Nickel foam can enhance the photocatalytic activity of TiO₂ during the thermo-photocatalytic process. Future studies should focus on the increase in ethylene adsorption on the photocatalyst surface because this is a crucial step for enhancing the yield of photocatalytic reactions.

Author Contributions: M.T.: investigation, data curation, formal analysis, writing—original draft preparation, visualisation; P.M.: investigation, data curation, formal analysis, writing—original draft preparation, visualisation; B.T.: conceptualisation, methodology, writing—review and editing, project administration. All authors have read and agreed to the published version of the manuscript.

Funding: This research was funded by the National Science Center, Poland, grant number 2020/39/B/ST8/01514. This work APC was supported by Rector of the West Pomeranian University of Technology in Szczecin for PhD students of the Doctoral School, grant number ZUT/14/2023.

Institutional Review Board Statement: Not applicable.

Informed Consent Statement: Not applicable.

Data Availability Statement: Data will be available in repozytorium ZUT.

Conflicts of Interest: The authors declare no conflicts of interest.

References

1. Pathak, N.; Caleb, O.J.; Geyer, M.; Herppich, W.B.; Rauh, C.; Mahajan, P.V. Photocatalytic and Photochemical Oxidation of Ethylene: Potential for Storage of Fresh Produce—A Review. *Food Bioprocess Technol.* **2017**, *10*, 982–1001. [[CrossRef](#)]
2. Elsgaard, L. Ethylene Removal by a Biofilter with Immobilized Bacteria. *Appl. Environ. Microbiol.* **1998**, *64*, 4168–4173. [[CrossRef](#)] [[PubMed](#)]
3. Keller, N.; Ducamp, M.-N.; Robert, D.; Keller, V. Ethylene Removal and Fresh Product Storage: A Challenge at the Frontiers of Chemistry. Toward an Approach by Photocatalytic Oxidation. *Chem. Rev.* **2013**, *113*, 5029–5070. [[CrossRef](#)] [[PubMed](#)]
4. Moghadam, H.Z.; Kheirkhah, B.; Kariminik, A. Ethylene Removal by Bio-filters in order to Increase Storage Life of Bananas. *Int. J. Life Sci.* **2015**, *9*, 62–65. [[CrossRef](#)]
5. Smith, A.W.J.; Poulston, S.; Rowsell, L.; Terry, L.A.; Anderson, J.A. A New Palladium-Based Ethylene Scavenger to Control Ethylene-Induced Ripening of Climacteric Fruit. *Platin. Met. Rev.* **2009**, *53*, 112–122. [[CrossRef](#)]
6. Martínez-Romero, D.; Bailén, G.; Serrano, M.; Guillén, F.; Valverde, J.M.; Zapata, P.; Castillo, S.; Valero, D. Tools to Maintain Postharvest Fruit and Vegetable Quality through the Inhibition of Ethylene Action: A Review. *Crit. Rev. Food Sci. Nutr.* **2007**, *47*, 543–560. [[CrossRef](#)] [[PubMed](#)]
7. Pathak, N.; Caleb, O.J.; Rauh, C.; Mahajan, P.V. Efficacy of photocatalysis and photolysis systems for the removal of ethylene under different storage conditions. *Postharvest Biol. Technol.* **2019**, *147*, 68–77. [[CrossRef](#)]
8. Hussain, M.; Bensaïd, S.; Geobaldo, F.; Saracco, G.; Russo, N. Photocatalytic Degradation of Ethylene Emitted by Fruits with TiO₂ Nanoparticles. *Ind. Eng. Chem. Res.* **2011**, *50*, 2536–2543. [[CrossRef](#)]
9. Parka, D.R.; Zhang, J.; Ikeue, K.; Yamashita, H.; Anpo, M. Photocatalytic Oxidation of Ethylene to CO₂ and H₂O on Ultrafine Powdered TiO₂ Photocatalysts in the Presence of O₂ and H₂O. *J. Catal.* **1999**, *185*, 114–119. [[CrossRef](#)]
10. Kumar, S.; Fedorov, A.G.; Gole, J.L. Photodegradation of ethylene using visible light responsive surfaces prepared from titania nanoparticle slurries. *Appl. Catal. B Environ.* **2005**, *57*, 93–107. [[CrossRef](#)]
11. Muramoto, Y.; Kimura, M.; Nouda, S. Development and future of ultraviolet light-emitting diodes: UV-LED will replace the UV lamp. *Semicond. Sci. Technol.* **2014**, *29*, 084004. [[CrossRef](#)]
12. Fonseca, J.d.M.; Miranda, S.M.; Monteiro, J.P.; Moreira, R.d.F.P.M.; Valencia, G.A.; Monteiro, A.R.; Vilar, V.J. Ethylene photocatalytic degradation using TiO₂ immobilized in a NETmix mini-photoreactor. *J. Environ. Chem. Eng.* **2023**, *11*, 110976. [[CrossRef](#)]
13. Shi, G.; Mahmood, A.; Lu, G.; Wang, X.; Tong, S.; Ge, M.; Xie, X.; Sun, J. Adsorption and Photodegradation of Acetaldehyde and Ethylene on TiO₂ (001) Surface: Experimental and First Principle Studies. *Catal. Lett.* **2019**, *149*, 2728–2738. [[CrossRef](#)]
14. Rychtowski, P.; Tryba, B.; Skrzypka, A.; Felczak, P.; Sreńscek-Nazzal, J.; Wróbel, R.J.; Nishiguchi, H.; Toyoda, M. Role of the Hydroxyl Groups Coordinated to TiO₂ Surface on the Photocatalytic Decomposition of Ethylene at Different Ambient Conditions. *Catalysts* **2022**, *12*, 386. [[CrossRef](#)]
15. Xia, J.; Dong, L.; Song, H.; Yang, J.; Zhu, X. Preparation of doped TiO₂ nanomaterials and their applications in photocatalysis. *Bull. Mater. Sci.* **2023**, *46*, 13. [[CrossRef](#)]
16. Bhattacharyya, K.; Varma, S.; Tripathi, A.K.; Bharadwaj, S.R.; Tyagi, A.K. Mechanistic Insight by *in Situ* FTIR for the Gas Phase Photo-oxidation of Ethylene by V-Doped Titania and Nano Titania. *J. Phys. Chem. B* **2009**, *113*, 5917–5928. [[CrossRef](#)] [[PubMed](#)]
17. Rao, Z.; Xie, X.; Wang, X.; Mahmood, A.; Tong, S.; Ge, M.; Sun, J. Defect Chemistry of Er³⁺-Doped TiO₂ and Its Photocatalytic Activity for the Degradation of Flowing Gas-Phase VOCs. *J. Phys. Chem. C* **2019**, *123*, 12321–12334. [[CrossRef](#)]
18. Zhang, Q.; Ye, S.; Chen, X.; Song, X.; Li, L.; Huang, X. Photocatalytic degradation of ethylene using titanium dioxide nanotube arrays with Ag and reduced graphene oxide irradiated by γ -ray radiolysis. *Appl. Catal. B Environ.* **2017**, *203*, 673–683. [[CrossRef](#)]
19. Lin, Y.-H.; Weng, C.-H.; Srivastava, A.L.; Lin, Y.-T.; Tzeng, J.-H. Facile Synthesis and Characterization of N-Doped TiO₂ Photocatalyst and Its Visible-Light Activity for Photo-Oxidation of Ethylene. *J. Nanomater.* **2015**, *2015*, 7. [[CrossRef](#)]
20. Lin, Y.-T.; Weng, C.-H.; Chen, F.-Y. Key operating parameters affecting photocatalytic activity of visible-light-induced C-doped TiO₂ catalyst for ethylene oxidation. *Chem. Eng. J.* **2014**, *248*, 175–183. [[CrossRef](#)]

21. Jo, W.-K.; Kang, H.-J. Aluminum sheet-based S-doped TiO₂ for photocatalytic decomposition of toxic organic vapors. *Chin. J. Catal.* **2014**, *35*, 1189–1195. [[CrossRef](#)]
22. Yang, H.; Yang, B.; Chen, W.; Yang, J. Preparation and Photocatalytic Activities of TiO₂-Based Composite Catalysts. *Catalysts* **2022**, *12*, 1263. [[CrossRef](#)]
23. Kajita, S.; Miyaguchi, K.; Tanaka, H.; Yasunaga, E.; Yoshida, T.; Ohno, N. Enhanced photocatalytic ethylene decomposition with anatase-rutile mixed nanostructures formed by He plasma treatment. *J. Photochem. Photobiol. A Chem.* **2021**, *418*, 113420. [[CrossRef](#)]
24. Mei, X.; Yuan, H.; Li, C. Study on the MOF Frame Pt-TiO₂ Hybrid Photocatalyst and Its Photocatalytic Performance. *Sustainability* **2023**, *15*, 1403. [[CrossRef](#)]
25. Chen, L.; Xie, X.; Song, X.; Luo, S.; Ye, S.; Situ, W. Photocatalytic degradation of ethylene in cold storage using the nanocomposite photocatalyst MIL101(Fe)-TiO₂-rGO. *Chem. Eng. J.* **2021**, *424*, 130407. [[CrossRef](#)]
26. Pugazhenthiran, N.; Valdés, H.; Mangalaraja, R.V.; Sathishkumar, P.; Murugesan, S. Graphene modified “black {0 0 1}TiO₂” nanosheets for photocatalytic oxidation of ethylene: The implications of chemical surface characteristics in the reaction mechanism. *Sep. Purif. Technol.* **2022**, *292*, 121008. [[CrossRef](#)]
27. Ji, B.; Zhao, W.; Duan, J.; Fu, L.; Ma, L.; Yang, Z. Immobilized Ag₃PO₄/GO on 3D nickel foam and its photocatalytic degradation of norfloxacin antibiotic under visible light. *RSC Adv.* **2020**, *10*, 4427–4435. [[CrossRef](#)]
28. Zhang, Q.; Li, F.; Chang, X.; He, D. Comparison of Nickel Foam/Ag-Supported ZnO, TiO₂, and WO₃ for Toluene Photodegradation. *Mater. Manuf. Process.* **2014**, *29*, 789–794. [[CrossRef](#)]
29. Yang, L.; Liu, Z.; Shi, J.; Hu, H.; Shangguan, W. Design consideration of photocatalytic oxidation reactors using TiO₂-coated foam nickels for degrading indoor gaseous formaldehyde. *Catal. Today* **2007**, *126*, 359–368. [[CrossRef](#)]
30. Hu, H.; Xiao, W.; Yuan, J.; Shi, J.; Shangguan, W. TiO₂/SiO₂ Composite Films Immobilized on Foam Nickel Substrate for the Photocatalytic Degradation of Gaseous Acetaldehyde. *Int. J. Photoenergy* **2008**, *2008*, 679421. [[CrossRef](#)]
31. Tryba, B.; Miadlicki, P.; Rychtowski, P.; Trzeciak, M.; Wróbel, R.J. The Superiority of TiO₂ Supported on Nickel Foam over Ni-Doped TiO₂ in the Photothermal Decomposition of Acetaldehyde. *Materials* **2023**, *16*, 5241. [[CrossRef](#)] [[PubMed](#)]
32. Hu, H.; Xiao, W.; Yuan, J.; Shi, J.; He, D.; Shangguan, W. High photocatalytic activity and stability for decomposition of gaseous acetaldehyde on TiO₂/Al₂O₃ composite films coated on foam nickel substrates by sol-gel processes. *J. Sol.-Gel Sci. Technol.* **2008**, *45*, 1–8. [[CrossRef](#)]
33. Tryba, B.; Orlikowski, J.; Wróbel, R.J.; Przepiórski, J.; Morawski, A.W. Preparation and Characterization of Rutile-Type TiO₂ Doped with Cu. *J. Mater. Eng. Perform.* **2015**, *24*, 1243–1252. [[CrossRef](#)]
34. Zeng, Q.; Xie, X.; Wang, X.; Wang, Y.; Lu, G.; Pui, D.Y.; Sun, J. Enhanced photocatalytic performance of Ag@TiO₂ for the gaseous acetaldehyde photodegradation under fluorescent lamp. *Chem. Eng. J.* **2018**, *341*, 83–92. [[CrossRef](#)]
35. Fu, X.; Clark, L.A.; Zeltner, W.A.; Anderson, M.A. Effects of reaction temperature and water vapor content on the heterogeneous photocatalytic oxidation of ethylene. *J. Photochem. Photobiol. A Chem.* **1996**, *97*, 181–186. [[CrossRef](#)]
36. Mphuthi, L.E.; Maseme, M.R.; Langner, E.H.G. Ti(IV)-Exchanged Nano-ZIF-8 and Nano-ZIF-67 for Enhanced Photocatalytic Oxidation of Hydroquinone. *J. Inorg. Organomet. Polym. Mater.* **2022**, *32*, 2664–2678. [[CrossRef](#)]
37. Ammawath, W.; Man, Y.C.; Baharin, B.; Rahman, R.A. A new method for determination of *tert*-butylhydroquinone (tbhq) in rbd palm olein with ftir spectroscopy. *J. Food Lipids* **2004**, *11*, 266–277. [[CrossRef](#)]
38. Fónagy, O.; Szabó-Bárdos, E.; Horváth, O. 1,4-Benzoquinone and 1,4-hydroquinone based determination of electron and superoxide radical formed in heterogeneous photocatalytic systems. *J. Photochem. Photobiol. A Chem.* **2021**, *407*, 113057. [[CrossRef](#)]

Disclaimer/Publisher’s Note: The statements, opinions and data contained in all publications are solely those of the individual author(s) and contributor(s) and not of MDPI and/or the editor(s). MDPI and/or the editor(s) disclaim responsibility for any injury to people or property resulting from any ideas, methods, instructions or products referred to in the content.